DOI: 10.48011/sbse.v1i1.2187

Linear quadratic regulator applied to low-frequency oscillation damping using the current sensitivity model

Elenilson de Vargas Fortes * **Marcus Vinícius Silvério Costa** **
Leonardo H. Macedo *** **Percival Bueno de Araujo** ***

* *Department of Academic Areas, Federal Institute of Education, Science, and Technology of Goiás, Jataí - GO (e-mail: elenilson.fortes@ifg.edu.br)*
** *Department of Engineering, Federal Rural University of the Semi-Arid Region, Caraúbas - RN (e-mail: marcus.costa@ufersa.edu.br)*
*** *Department of Electrical Engineering, São Paulo State University, Ilha Solteira - SP (e-mails: leohfmp@ieee.org, percival@dee.feis.unesp.br)*

Abstract: This paper proposes the use of the linear quadratic regulator, a systematic method in which the controller is obtained by minimizing a quadratic performance index, to ensure the desired damping rates of the low-frequency oscillatory modes present in an electrical power system. The current sensitivity model is used to represent the dynamics of the system. To validate the proposed technique, simulations were carried out using a single machine infinite bus system. From the results obtained, it was evidenced the excellent performance of the proposed controller, since it was able to damp the low-frequency oscillatory mode present in the test system, accrediting it as a powerful tool in the study and analysis of small-signal stability in electric power systems.

Keywords: Current sensitivity model; linear quadratic regulator; local modes of oscillation; small-signal stability; electric power systems.

1. INTRODUCTION

According to data from the national interconnected system, more than 96% of the Brazilian electric power transmission network is interconnected. Interconnected power systems are a reality in the current conjuncture, not only in the national scenario but also globally. There are some advantages and disadvantages of having an interconnected transmission system. As an advantage, it can be mentioned the fact that if any eventuality occurs with any generating unit, the system may have its demands supplied by other generating units. As a disadvantage, interconnected power systems are usually characterized by long transmission lines, with high impedance values, which may favor the emergence of low-frequency electromechanical oscillations (Fortes et al., 2016).

Low-frequency oscillations can be classified according to their frequency of occurrence and are usually classified as local or interarea modes. Local modes occur within a range of 0.80 to 2.00 Hz, while interarea modes occur within a range of 0.20 to 0.80 Hz (Kundur, 1994; Sauer and Pai, 1998; Larsen and Swann, 1981).

The presence of these oscillatory modes in a power system may compromise its operation and, in some cases, cause the system to collapse. Therefore, control techniques should be implemented to damp these low-frequency electromechanical oscillations (Fortes et al., 2016).

Power system stabilizers (PSS) and power oscillation damping (POD) controllers coupled to automatic voltage regulators (AVR) (Anderson and Fouad, 1993; Kundur, 1994) and flexible ac transmission system (FACTS) devices (Hingorani and Gyugyi, 1999; Sen and Sen, 2009; Fortes et al., 2016; Fortes et al., 2017), respectively, can damp both the local (PSS) and interarea (FACTS-POD) oscillatory modes present in the system.

Several optimization techniques have been successfully used for tuning the parameters of the PSS and FACTS-POD controllers. Metaheuristics, such as the Chu-Beasley's genetic algorithm, variable neighborhood search, artificial bee colony algorithm, and novel bat algorithm, are some examples that can be cited (Fortes et al., 2016; Martins et al., 2017; Fortes et al., 2018; Miotto et al., 2018).

On the other hand, the concept of state feedback control is already known and widely addressed in the literature (Ogata, 2010). Applications in the context of wind power generation are some examples of the use of this technique (Costa et al., 2010; Pinto et al., 2012; Costa et al., 2012). Recently, control techniques, such as the linear quadratic regulator (LQR), have been used in studies related to the stability of power systems (Jokarzadeh et al., 2019) using the Heffron and Phillips (1952) model. It can be observed

that the study of the application of state-space control techniques is modern and current, with the potential to be explored in studies related to the stability of power systems using alternative modeling, such as the current sensitivity model (CSM) Takahashi et al. (2018).

Different from the proposal presented by Jokarzadeh et al. (2019) and as one of the main contributions of this work, it is proposed the application of the LQR controller with the CSM for the single machine infinite bus (SMIB) system acting on the AVR through state feedback. For the LQR controller in the state-space applied to the CSM, the choice of the weighting matrices is made by tuning the matrices Q_c and R_c of the Riccati equation (Ogata, 2010) applied to the CSM (Takahashi et al., 2018), as presented in Section 3.

The remainder of this work is organized as follows: Section 2 presents the CSM, with theoretical concepts of the CSM applied to SMIB system; Section 3 presents the proposed control strategy, in which the LQR theory is presented, as well as the proposed application of the LQR to the AVR model; Section 4 presents the results for the tests, comparing the system before and after the compensation; finally, Section 5 presents the conclusions of the work and suggestions for future works.

2. CURRENT SENSITIVITY MODEL

2.1 Basic Equations of the CSM

Fig. 1 shows a salient pole synchronous generator G connected to an infinite bus, represented by ∞, through a transmission line with impedance $\bar{Z}_e$, in which a current $\mathbf{I}$ circulates.

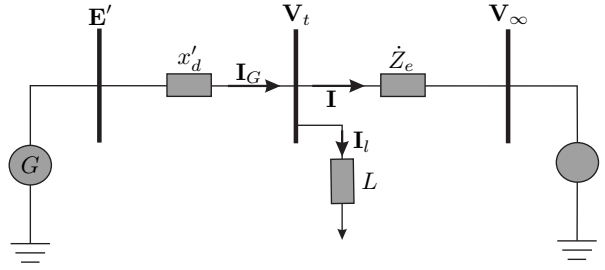

Figure 1. Single-line diagram of the SMIB system.

In Fig. 1, $\mathbf{E}'$, $\mathbf{V}_t$, and $\mathbf{V}_\infty$ are, respectively, the internal voltage, the terminal voltage of the synchronous generator G, and the voltage at the infinite bus. In addition, x'_d is the direct axis transient reactance of generator G, $\mathbf{I}_G$ is the current delivered by generator G at bus t, and $\mathbf{I}_l$ is the current drained by the load connected to bus t.

From Fig. 1, through inspection, it is possible to obtain (1)−(4).

$$V_d = V\sin(\delta-\theta) \tag{1}$$

$$V_q = V\cos(\delta-\theta) \tag{2}$$

$$I_d = \frac{E'_q - V_q}{x'_d} \tag{3}$$

$$I_q = \frac{V_q}{x_q} \tag{4}$$

In (1)−(4), x_q is the quadrature axis transient reactance of generator G, δ is internal angle of generator G, and θ is the voltage angle at bus t. In addition, E'_q, V_q, and V_d are, respectively, the quadrature axis internal voltage, the in-phase voltage, and the quadrature axis voltage of generator G (Anderson and Fouad, 1993).

2.2 Currents Generated by the Synchronous Machine

By applying the transformation matrix (Anderson and Fouad, 1993) to (3) and (4), (5) and (6) are obtained.

$$I_{G_r} = \sin(\delta)\left(\frac{E'_q - V_q}{x'_d}\right) + \cos(\delta)\left(\frac{V_d}{x_q}\right) \tag{5}$$

$$I_{G_m} = -\cos(\delta)\left(\frac{E'_q - V_q}{x'_d}\right) + \sin(\delta)\left(\frac{V_d}{x_q}\right) \tag{6}$$

In (5) and (6), I_{G_r} and I_{G_m} are, respectively, the real and imaginary components of the current of the synchronous generator G.

2.3 Current on the Transmission Line

To calculate the current $\mathbf{I}$, that circulates between the terminal bus of the generator and the infinite bus (see Fig. 1), consider $\dot{Z}_e = r_e + jx_e$ and $\mathbf{V}_t = V\cos(\theta) + jV\sin(\theta)$.

By analyzing Fig. 1, (7) and (8) are obtained.

$$I_r = \frac{r_e(V\cos(\theta) - V_\infty) + x_e V\sin(\theta)}{|\dot{Z}_e|^2} \tag{7}$$

$$I_m = \frac{r_e V\sin(\theta) - x_e(V\cos(\theta) - V_\infty)}{|\dot{Z}_e|^2} \tag{8}$$

Equations (7) and (8) represent, respectively, the real and imaginary components of the current that circulates on the line connecting the terminal bus of the generator and the infinite bus.

2.4 Load Currents

Considering the existence of a load connected to the terminal bus of the generator (see Fig. 1) which demands a complex power $\dot{S}_l = P_l + jQ_l$, it is possible, by inspection, to obtain the current ($\mathbf{I}_l$) as presented in (9) and (10).

$$I_{l_r} = \frac{P_l\cos(\theta) + Q_l\sin(\theta)}{V} \tag{9}$$

$$I_{l_m} = -\left(\frac{Q_l\cos(\theta) - P_l\sin(\theta)}{V}\right) \tag{10}$$

Equations (9) and (10) represent, respectively, the real and imaginary components of the current demanded by a load connected at the terminal bus of the generator.

2.5 Nodal Current Balance in the SMIB System

The fundamental principle of the CSM is to apply the nodal current balance to each bus of the system. Mathematically, the current balance can be defined as shown in (11) and (12).

$$\mathbf{I}_{G_r} - \mathbf{I}_r - \mathbf{I}_{l_r} = 0 \tag{11}$$

$$\mathbf{I}_{G_m} - \mathbf{I}_m - \mathbf{I}_{l_m} = 0 \tag{12}$$

Equations (11) and (12) are algebraic expressions that represent, in their fundamental form, the nodal balance of currents at the terminal bus of the generator.

2.6 Internal Voltage of the Synchronous Machine

According to Kundur (1994), the variations of the internal voltage of the synchronous machine are expressed by (13).

$$\dot{E}'_q = \frac{1}{T'_{d_0}}\left[E_{fd} - \frac{x_d}{x'_d}E'_q + \left(\frac{x_d}{x'_d} - 1\right)V\cos(\delta - \theta)\right] \quad (13)$$

In (13), T'_{d_0} is the transient direct axis open-circuit time constant, E_{fd} represents the excitation voltage of the synchronous machine, and x_d is the direct axis transient synchronous reactance of the generator.

2.7 Field Voltage of the Synchronous Machine

To consider the effects of the field winding of the synchronous machine in the model, the generator must be equipped with an AVR (Anderson and Fouad, 1993). In this work, a first-order AVR is used to represent the variation of the excitation voltage of the synchronous machine, as it can be observed in Fig. 2.

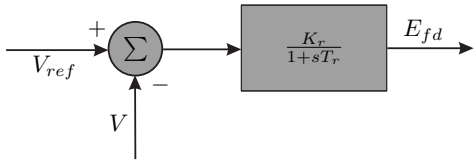

Figure 2. Block diagram of the AVR.

By analyzing Fig. 2 it is possible to obtain (14). This equation represents the field voltage in the time domain.

$$\dot{E}_{fd} = -\frac{1}{T_r}E_{fd} + \frac{K_r}{T_r}V_{ref} - \frac{K_r}{T_r}V \quad (14)$$

In (14), K_r and T_r are, respectively, the gain and time constant of the AVR and V_{ref} is the reference voltage of the generator.

2.8 Electromechanical Equations

For a complete representation of the SMIB system, it is necessary to describe the mechanical quantities of the synchronous machine, i.e., the angular velocity of its rotor (ω) and its internal angle (δ).

According to Demello and Concordia (1969) the electromechanical equations of the generator are represented in (15) and (16).

$$\dot{\omega} = \frac{1}{M}(P_m - P_G - D\omega) \quad (15)$$

$$\dot{\delta} = \omega_0\omega \quad (16)$$

In (15) and (16), $M = 2H$ and represents the inertia constant of the generator, P_m is the mechanical input power, P_G is the active power generated by the synchronous machine, D is the damping torque coefficient of the electromechanical loop, and $\omega_0 = 377$ rad/s.

2.9 Time Domain Representation of the SMIB system through the CSM

As presented in Subsections 2.1−2.8, the CSM is used to represent a set of differential equations, (5)−(10) and (13)−(16) as well as algebraic equations, (11) and (12), which model the system's dynamics. The CSM preserves the external network, facilitates the inclusion of new devices in the system, and preserves the terminal bus of the generator, characteristics that are not present in the model of Heffron and Phillips (1952), that are determining points for choosing the CSM.

By admitting small variations around an equilibrium point, (5)−(16) can be linearized and, therefore, represented as shown in (17)−(20).

$$\Delta x = \left[\Delta\omega \;\; \Delta\delta \;\; \Delta E'_q \;\; \Delta E_{fd}\right]^t \quad (17)$$

$$\Delta u = \left[\Delta P_m \;\; \Delta V_{ref} \;\; \Delta P_l \;\; \Delta Q_l\right]^t \quad (18)$$

$$\Delta z = \left[\Delta\theta \;\; \Delta V\right]^t \quad (19)$$

$$\begin{bmatrix}\Delta\dot{x}\\ 0\end{bmatrix} = \begin{bmatrix}J1 & J2\\ J3 & J4\end{bmatrix}\begin{bmatrix}\Delta x\\ \Delta z\end{bmatrix} + \begin{bmatrix}B1\\ B2\end{bmatrix}[\,\Delta u\,] \quad (20)$$

In (17)−(19), the state variables are represented by Δx, the input represented by Δu, and the algebraic variables by Δz. In addition, $J1$, $J2$, $J3$, $J4$, $B1$, and $B2$ are described in (21)−(23).

$$J1 = \begin{bmatrix} -\frac{D}{M} & -\frac{K1}{M} & -\frac{K2}{M} & 0\\ \omega_0 & 0 & 0 & 0\\ 0 & -\frac{KA}{T'_{d_0}} & -\frac{x_d}{x'_d T'_{d_0}} & \frac{1}{T'_{d_0}}\\ 0 & 0 & 0 & -\frac{1}{T_r}\end{bmatrix} \quad J2 = \begin{bmatrix}\frac{K1}{M} & \frac{K3}{M}\\ 0 & 0\\ \frac{KA}{T'_{d_0}} & \frac{KV}{T'_{d_0}}\\ 0 & -\frac{K_r}{T_r}\end{bmatrix} \quad (21)$$

$$J3 = \begin{bmatrix}0 & R2_G & R1_G & 0\\ 0 & M2_G & M1_G & 0\end{bmatrix} \qquad J4 = \begin{bmatrix}A_r & B_r\\ A_m & B_m\end{bmatrix} \quad (22)$$

$$B1 = \begin{bmatrix}\frac{1}{M} & 0 & 0 & 0\\ 0 & 0 & 0 & 0\\ 0 & 0 & 0 & 0\\ 0 & \frac{K_r}{T_r} & 0 & 0\end{bmatrix} \quad B2 = \begin{bmatrix}0 & 0 & -C3_r & -C4_r\\ 0 & 0 & -C3_m & -C4_m\end{bmatrix} \quad (23)$$

Equation (20) can be rearranged as shown in (24).

$$\Delta\dot{x} = A\Delta x + B\Delta u \quad (24)$$

In (24), the matrix $A = (J1 - J2J4^{-1}J3)$ is the state matrix and $B = (B1 - J2J4^{-1}B2)$ is the input matrix. More information on the coefficients shown in (21)−(23) can be found in Appendix A.

3. CONTROL STRATEGY

The LQR is a systematic method in which the controller is obtained by minimizing the quadratic performance index. According to Ogata (2010), this regulator is defined by (25).

$$J_\infty(x,u,t) = \int_0^\infty \left[x^T(t)\,Q_c\,x(t) + u^T(t)\,R_c\,u(t)\right]dt \quad (25)$$

In (25), $Q_c = {Q_c}^T \geq 0$ and $R_c = {R_c}^T > 0$ are real weighting matrices that can be adjusted to improve performance of the system.

In this paper, the state-space model is represented by (26).

$$\Delta\dot{x} = A\Delta x + B_{V_S}u_{Vs} + B\Delta u \quad (26)$$

In (26), B_{Vs} is the state space vector obtained from (14) and the AVR shown in Fig. 2, being defined in (27).

The signal Δu is an exogenous disturbance to the system represented via the CSM. Therefore, the AVR modeled in the state space aims to guarantee the damping of these disturbances for the stabilization of the synchronous generator.

$$B_{Vs} = \begin{bmatrix} 0 & 0 & 0 & \frac{K_r}{T_r} \end{bmatrix}^T \tag{27}$$

To stabilize the SMIB system in the state space, consider that the control signal u_{Vs} is defined as shown in (28).

$$u_{Vs} = -K_{LQR}\Delta\dot{x} \tag{28}$$

In (28), the gain K_{LQR} is obtained by solving the Riccati equation (29) and (30) (Ogata, 2010).

$$A^T P + PA + Q_c - (PB_{V_S})^T R_c^{-1}(PB_{V_S}) = 0 \tag{29}$$

$$K_{LQR} = R_c^{-1} B_{Vs}^T P \tag{30}$$

Fig. 3 illustrates the proposed block diagram for the state feedback control of the AVR, hereinafter referred to as the state space automatic voltage regulator (SS-AVR), conceived from Fig. 2.

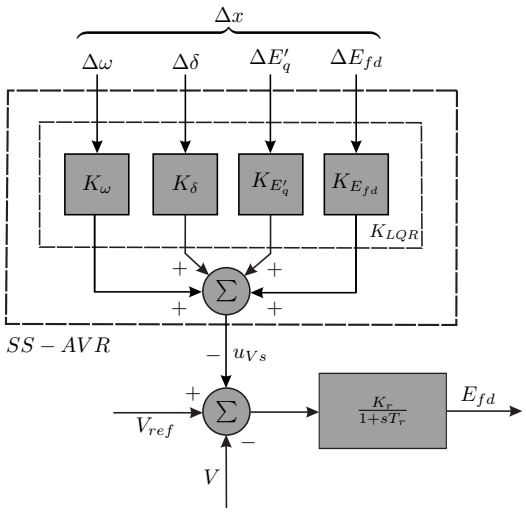

Figure 3. Block diagram of the proposed control strategy.

By analyzing Fig. 3 it is concluded that the state variables are essential parameters for the design of the LQR controller. The SS-AVR representation presented on Fig. 3 is based on the state feedback in (28), in which the gains are directly associated with the state variables Δx.

4. TESTS AND RESULTS

The simulations were carried out in a SMIB system, which data is shown in Table B.1 of Appendix B. Initially, the SMIB system is simulated as modeled in Section 2 and the eigenvalue of interest is $\lambda_i = 0.3190 \pm j7.2773$, with $\omega_n = 1.15$ Hz, and $\xi_i = -0.04$, in which ω_n is the frequency value, and ξ_i is the damping value for the eigenvalue of interest in the SMIB system before the compensation.

It can be verified that the system has eigenvalues with positive real part for the given operating point, which characterizes the test system as unstable.

For the operation of the system to become stable, the control strategy presented in Section 3 is used, where (31) and (32) are obtained.

$$K_{LQR} = \begin{bmatrix} -8.14 \times 10^4 \\ -3.99 \times 10^4 \\ 3.73 \times 10^1 \\ 4.30 \times 10^{-3} \end{bmatrix}^T \tag{31}$$

$$B_{Vs} = \begin{bmatrix} 0 & 0 & 0 & 2 \times 10^5 \end{bmatrix}^T \tag{32}$$

In (31) the numerical gains of the LQR controller, obtained by state feedback from (29) and (30), are shown, while (32) is the numerical vector of the states obtained from (27), in which $Q_c = diag(1, 1, 1, 0)$ and $R_c = 1$ were obtained experimentally.

After adopting the control parameters shown in (31) and (32), the SMIB system is tested again, and the results of the simulation for the system compensated by the LQR controller are as follows: the eigenvalue of interest is $\lambda_i = -3.7912 \pm j8.2150$, with $\omega_n = 1.44$ Hz, and $\xi_i = 0.41$.

One of the inherent advantages of the LQR control is the systematic stabilization process based on the weighting matrices. By analyzing the results, it can be verified that the inherent characteristics of the proposed LQR, in (29) and (30), ensured the stabilization of the test system with the value of the frequency of the dominant eigenvalue of the compensated system close to the same value in the system before the compensation, in the left side of the complex plane and highly damped.

Fig. 4 shows the time response of the compensated system, with a constant perturbation in ΔP_m of 0.05 p.u. from the time $t = 300$ ms.

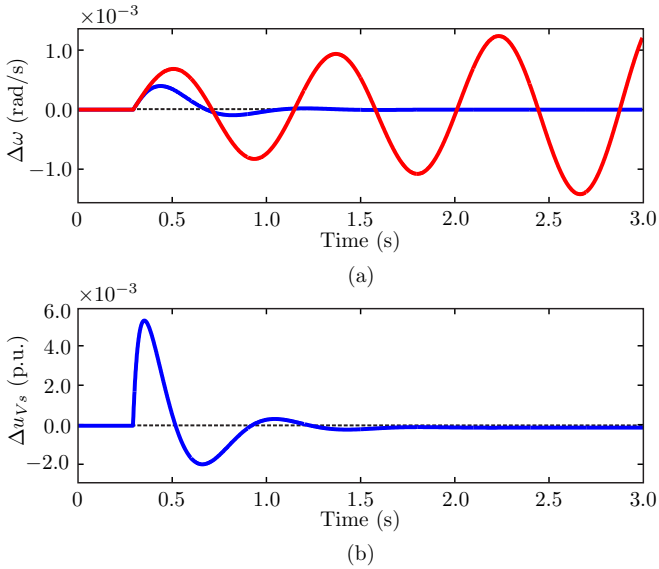

Figure 4. Time response of the compensated LQR model: (a) variation of the angular velocity of the synchronous generator and (b) variation of the control signal of the actuator.

By looking at Fig. 4 (a), it can be verified that the red curve is characterized by increasing amplitudes after the disturbance of 0.05 p.u. on the mechanical power of the synchronous machine. This was expected since in this case, the SMIB system was unstable. After using the LQR control, the system becomes stable, with a peak value of 3.98×10^{-4} rad/s, as evidenced by the blue curve, demonstrating a high margin of stability at small disturbances (0.41 p.u. of damping). In Fig. 4 (b), it can be

seen that the control signal Δu_{Vs} has a peak value of 5.35×10^{-3} p.u. at $t = 360$ ms, showing that the control strategy adopted in this work guarantees the stabilization of the system with smooth action of the control signal, without compromising the operating conditions of the generator.

5. CONCLUSION

In this work, the linear quadratic regulator (LQR) was used to provide a control signal to stabilize a single machine infinite bus system. To model the dynamics of the electric power system, the current sensitivity model (CSM) was used.

By analyzing the obtained results, it was observed that the system compensated by the proposed controller, via state feedback for the automatic voltage regulator, demonstrated efficiency in the system stabilization. The analysis of the obtained results allows concluding that the LQR can be accredited as a powerful tool in the study of small-signal stability of electric power systems.

As future work proposal, the feasibility of applying the LQR with the CSM for small-signal stability studies in multi-machine systems will be verified. For the studies related to new control strategies, it will be verified the feasibility of using the LQR applied to the CSM optimized by heuristic methods.

ACKNOWLEDGMENT

This work was supported by the Coordination for the Improvement of Higher Education Personnel (CAPES) – Finance Code 001, the Federal Rural University of the Semi-Arid Region (UFERSA), the Federal Institute of Education, Science, and Technology of Goiás (IFG), and the São Paulo Research Foundation (FAPESP), under grants 2018/20355-1 and 2019/19632-3.

REFERENCES

Anderson, P. and Fouad, A.A. (1993). *Power system control and stability*. Wiley-IEEE Press, New York.

Costa, M.V.S., Pinto, V.P., Campos, J.C.T., and Nascimento, J.A. (2012). Controle por D-alocação robusta via LMI aplicado em sistemas de geração eólica. In *IV Simpósio Brasileiro de Sistemas Elétricos*, 1–6.

Costa, M.V.S., Pinto, V.P., Campos, J.C.T., and Reis, L.L.N. (2010). Modelagem, simulação e controle ótimo de geradores eólicos interligados ao sistema de distribuição de energia elétrica. In *III Simpósio Brasileiro de Sistemas Elétricos*, 1–6.

Demello, F.P. and Concordia, C. (1969). Concepts of synchronous machine stability as affected by excitation control. *IEEE Transactions on Power Apparatus and Systems*, PAS-88(4), 316–329. doi:10.1109/TPAS.1969.292452.

Fortes, E.V., Araujo, P.B., and Macedo, L.H. (2016). Coordinated tuning of the parameters of PI, PSS and POD controllers using a specialized Chu-Beasley's genetic algorithm. *Electric Power Systems Research*, 140, 708–721. doi:10.1016/j.epsr.2016.04.019.

Fortes, E.V., Araujo, P.B., Macedo, L.H., Gamino, B.R., and Martins, L.F.B. (2016). Analysis of the influence of PSS and IPFC-POD controllers in small-signal stability using a simulated annealing algorithm. In *2016 12th IEEE International Conference on Industry Applications (INDUSCON)*, 1–8. doi:10.1109/INDUSCON.2016.7874512.

Fortes, E.V., Macedo, L.H., Araujo, P.B., and Romero, R. (2018). A VNS algorithm for the design of supplementary damping controllers for small-signal stability analysis. *International Journal of Electrical Power & Energy Systems*, 94, 41 – 56. doi:10.1016/j.ijepes.2017.06.017.

Fortes, E.V., Macedo, L.H., Martins, L.F.B., and Miotto, E.L. (2017). A fireworks metaheuristic for the design of PSS and TCSC-POD controllers for small-signal stability studies. In *Latin American Congress on Generation, Transmission and Distribution (CLAGTEE)*, 1–6. Mar del Plata - AG.

Heffron, W.G. and Phillips, R.A. (1952). Effect of a modern amplidyne voltage regulator on underexcited operation of large turbine generators. *Transactions of the American Institute of Electrical Engineers. Part III: Power Apparatus and Systems*, 71(1), 692–697.

Hingorani, N.G. and Gyugyi, L. (1999). *Understanding FACTS: concepts and technology of flexible ac transmission system*. IEEE, New York.

Jokarzadeh, M., Abedini, M., and Seifi, A. (2019). Improving power system damping using a combination of optimal control theory and differential evolution algorithm. *ISA Transactions*, 90, 169–177. doi:10.1016/j.isatra.2018.12.039.

Kundur, P. (1994). *Power system stability and control*. McGraw-Hill, New York.

Larsen, E.V. and Swann, D.A. (1981). Applying power system stabilizers part II: performance objectives and tuning concepts. *IEEE Transactions on Power Apparatus and Systems*, PAS-100(6), 3025–3033. doi:10.1109/TPAS.1981.316410.

Martins, L.F.B., Araujo, P.B., de Fortes, E.V., and Macedo, L.H. (2017). Design of the PI–UPFC–POD and PSS damping controllers using an artificial bee colony algorithm. *Journal of Control, Automation and Electrical Systems*, 28(6), 762–773. doi:10.1007/s40313-017-0341-z.

Miotto, E.L., Araujo, P.B., Fortes, E.V., Gamino, B.R., and Martins, L.F.B. (2018). Coordinated tuning of the parameters of PSS and POD controllers using bioinspired algorithms. *IEEE Transactions on Industry Applications*, 54(4), 3845–3857. doi:10.1109/TIA.2018.2824249.

Ogata, K. (2010). *Engenharia do controle moderno*. Person Prentice Hall, São Paulo, 5 edition.

Pinto, V.P., Campos, J.C.T., Costa, M.V.S., and Silva Junior, A. (2012). Servomecanismo robusto multivariável aplicado em sistema de geração eólica. In *10th IEEE/IAS International Conference on Industry Applications INDUSCON*, 1–6.

Sauer, P.W. and Pai, M.A. (1998). *Power system dynamics and stability*. Prentice Hall, New Jersey.

Sen, K. and Sen, M. (2009). *Introduction to FACTS controllers: theory, modeling, and applications*. IEEE Press-John Wiley, New Jersey.

Takahashi, A.L.M., Fortes, E.V., Araujo, P.B., Miotto, E.L., and Martins, L.F.B. (2018). A current sensi-

tivity model for power system stability studies. In *2018 13th IEEE International Conference on Industry Applications (INDUSCON)*, 955–962. doi:10.1109/INDUSCON.2018.8627348.

Appendix A. COEFFICIENTS OF THE CSM FOR THE SMIB SYSTEM

$$K1 = \frac{\partial P_G}{\partial \delta} = \frac{V}{x'_d}\cos(\delta-\theta)\cdot E'_q + V^2\cos(2\delta-2\theta)\left(-\frac{1}{x'_d}+\frac{1}{x_q}\right) \tag{A.1}$$

$$K2 = \frac{\partial P_G}{\partial E'_q} = \frac{V}{x'_d}\sin(\delta-\theta) \tag{A.2}$$

$$K3 = \frac{\partial P_G}{\partial V} = \frac{\sin(\delta-\theta)\cdot E'_q}{x'_d} + V\sin(2\delta-2\theta)\left(-\frac{1}{x'_d}+\frac{1}{x_q}\right) \tag{A.3}$$

$$KA = \frac{\partial E'_q}{\partial \theta} = V\left(\frac{x_d - x'_d}{x'_d}\right)\sin(\delta-\theta) \tag{A.4}$$

$$KV = \frac{\partial E'_q}{\partial V} = \left(\frac{x_d - x'_d}{x'_d}\right)\cos(\delta-\theta) \tag{A.5}$$

$$R1_G = \frac{\partial I_{G_r}}{\partial E'_q} = \frac{1}{x'_d}\sin(\delta) \tag{A.6}$$

$$R2_G = \frac{\partial I_{G_r}}{\partial \delta} = \frac{1}{x'_d}E'_q\cos(\delta) + \left(\frac{1}{x_q}-\frac{1}{x'_d}\right)V\cos(2\delta-\theta) \tag{A.7}$$

$$R3_G = \frac{\partial I_{G_r}}{\partial V} = -\frac{1}{x'_d}\sin(\delta)\cos(\delta-\theta) + \frac{1}{x_q}\cos(\delta)\sin(\delta-\theta) \tag{A.8}$$

$$R4_G = \frac{\partial I_{G_r}}{\partial \theta} = -\frac{1}{x'_d}V\sin(\delta)\sin(\delta-\theta) - \frac{1}{x_q}V\cos(\delta)\cos(\delta-\theta) \tag{A.9}$$

$$M1_G = \frac{\partial I_{G_m}}{\partial E'_q} = -\frac{1}{x'_d}\cos(\delta) \tag{A.10}$$

$$M2_G = \frac{\partial I_{G_m}}{\partial \delta} = \frac{1}{x'_d}E'_q\sin(\delta) + \left(\frac{1}{x_q}-\frac{1}{x'_d}\right)V\sin(2\delta-\theta) \tag{A.11}$$

$$M3_G = \frac{\partial I_{G_m}}{\partial V} = \frac{1}{x'_d}\cos(\delta)\cos(\delta-\theta) + \frac{1}{x_q}\sin(\delta)\sin(\delta-\theta) \tag{A.12}$$

$$M4_G = \frac{\partial I_{G_m}}{\partial \theta} = \frac{V}{x'_d}\cos(\delta)\sin(\delta-\theta) - \frac{V}{x_q}\sin(\delta)\cos(\delta-\theta) \tag{A.13}$$

$$R1 = \frac{\partial I_r}{\partial V} = \frac{1}{|\dot{Z}_e|^2}\left[r_e\cos(\theta) + x_e\sin(\theta)\right] \tag{A.14}$$

$$R2 = \frac{\partial I_r}{\partial \theta} = -\frac{V}{|\dot{Z}_e|^2}\left[r_e\sin(\theta) - x_e\cos(\theta)\right] \tag{A.15}$$

$$M1 = \frac{\partial I_m}{\partial V} = \frac{1}{|\dot{Z}_e|^2}\left[r_e\sin(\theta) - x_e\cos(\theta)\right] \tag{A.16}$$

$$M2 = \frac{\partial I_m}{\partial \theta} = \frac{V}{|\dot{Z}_e|^2}\left[r_e\cos(\theta) + x_e\sin(\theta)\right] \tag{A.17}$$

$$C1_r = \frac{\partial I_{l_r}}{\partial \theta} = -\left(\frac{P_l\sin(\theta) - Q_l\cos(\theta)}{V}\right) \tag{A.18}$$

$$C2_r = \frac{\partial I_{l_r}}{\partial V} = -\left(\frac{P_l\cos(\theta) + Q_l\sin(\theta)}{V^2}\right) \tag{A.19}$$

$$M1_r = \frac{\partial I_{l_m}}{\partial \theta} = \frac{P_l\cos(\theta) + Q_l\sin(\theta)}{V} \tag{A.20}$$

$$M2_r = \frac{\partial I_{l_m}}{\partial V} = -\left(\frac{P_l\sin(\theta) - Q_l\cos(\theta)}{V^2}\right) \tag{A.21}$$

$$A_r = R4_G - R2 - C1_r \tag{A.22}$$

$$B_r = R3_G - R1 - C2_r \tag{A.23}$$

$$A_m = M4_G - M2 - C1_m \tag{A.24}$$

$$B_m = M3_G - M1 - C2_m \tag{A.25}$$

Appendix B. PARAMETERS OF THE SMIB SYSTEM

Table B.1. Parameters of the SMIB system

Parameters	Value	Unity
H	5	kgm^2
D	0	kW· s/kVA
T'_{d_0}	6	s
$\|\mathbf{V}_t\|$	1.0	p.u.
P_l	0	p.u.
Q_l	0	p.u.
K_r	40	p.u.
T_r	0.001	s
x'_d	0.32	p.u.
x_d	1.6	p.u.
x_q	1.55	p.u.
r_e	0	p.u.
x_e	0.30	p.u.